PHGN 326 - Advanced Physics Lab II

LAB #3: Neutron Activation

Brennan Fieck
PH326 Section B Lab Group R-11
Experiment Date: 2nd of March, 2017
Report Due Date: 9th of February, 2017

Abstract

In this lab values for the half-lives of radioactive isotopes $^{28}_{12}$Mg and $^{28}_{13}$Al were calculated from data obtained by measuring the net area of the photo-peaks of these isotopes. The isotopes were created by bombarding ordinary samples of $^{27}_{13}$Al with neutrons of different energies and half-lives were determined by measuring how the photo-peaks changed as time wore on. Measurements were taken by connecting a photo-multiplier tube to a multi-channel analyzer which was polled by Maestro®data collection software. The values calculated are compared to the accepted values in Table 1.

Isotope	**Experimentally-Determined Half-Life (seconds)**	**Accepted Half-Life (seconds)**
$^{28}_{13}$Al	592 ±30.4	567.48
$^{27}_{12}$Mg	145 ±13.6	134.484

Tab. 1: Experimental Values Compared to Accepted Values

Grade	Score	Available
Abstract and Cover Pg.		5
Fig. & Plt.		10
Data & Error Ana.		10
Writing		10
Total		35

1 Introduction

The task in this lab was to determine the half-lives of radioactive specimens that are produced by bombarding aluminum with neutrons. This "activates" the aluminum which then either becomes a heavier isotope of aluminum in the process

$$^{27}_{13}\mathrm{Al} +^{1}_{0} n \rightarrow^{28}_{13} \mathrm{Al}$$

which quickly decays via β^- and γ decay modes or transmutes into an isotope of magnesium in the process

$$^{27}_{13}\mathrm{Al} +^{1}_{0} n \rightarrow^{1}_{1} p +^{27}_{12} \mathrm{Mg}$$

which itself decays via β^- and γ decay modes relatively quickly. By measuring the rate at which the photo-peaks corresponding to these decay modes reduced to background noise, a calculation of each species' half life was obtained.

2 Apparatus

2.1 Layout

The lab's apparatus occupied only two distinct configurations during the course of all data collection, which varied only in the distances between the source and PMT. For calibration the sources were held some arbitrary distance away, and for actual data collection the sources were placed as close to the detector as possible, as shown in Figure 1.

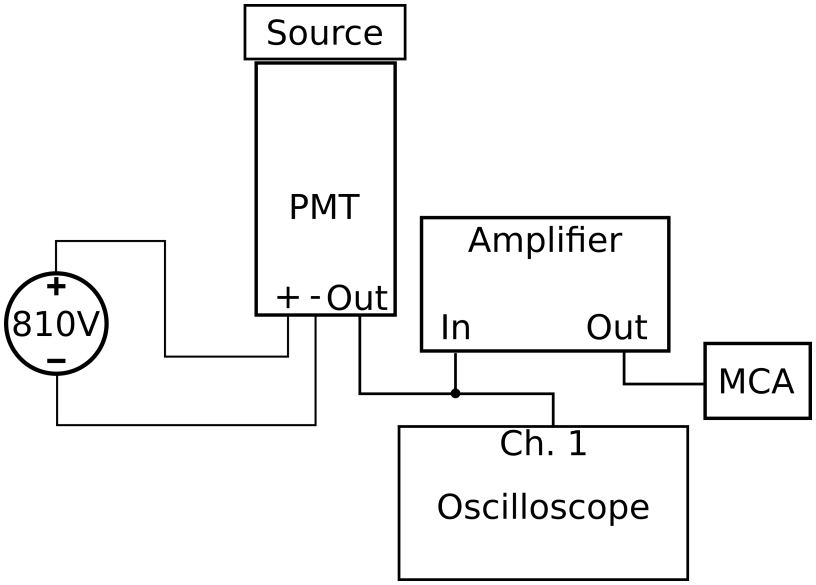

Fig. 1: Basic Illustration of Lab Setup

As shown, the lab utilized a Photomultiplier Tube (PMT) to count incident photons, and generating a signal which was captured both directly and after amplification by the Oscilloscope or Maestro®software through the Multi-Channel Analyzer (MCA).

2.2 Sources

The sources used in this lab were as follows:

- $^{137}\mathrm{Cs}$
- $^{60}\mathrm{Co}$
- Cylindrical Activated Al
- Trapezoidal Activated Al

Measurements later in the report will indicate which source was used. The ^{137}Cs and ^{60}Co sources were used solely for calibration of the data collection software, as described in Section 3.1. Both activated aluminum sources are large pieces of aluminum (that is, larger than the detector's face) which have been bombarded by neutrons to induce the production of radioactive isotopes. The two isotopes of interest for this lab are $^{27}_{12}$Mg and $^{28}_{13}$Al. When a neutron impacts an otherwise stable atom, it can be directly absorbed into the nucleus which then decays via $\beta^{\pm}$ or γ radiation. In the case of the aluminum being activated, this reaction is

$$^{27}_{13}\text{Al} +^{1}_{0} n \rightarrow^{28}_{13} \text{Al}.$$

On the other hand, if the energy of the incident neutron is great enough, it can cause the ejection of another nucleon simultaneously. If the ejected nucleon happens to be a proton, the nucleus is transmuted (if the ejected nucleon is a neutron nothing has really changed). In the case of activating aluminum, the process is

$$^{27}_{13}\text{Al} +^{1}_{0} n \rightarrow^{1}_{1} p +^{27}_{12} \text{Mg}.$$

In order to provide easily-detectable photo-peaks for each isotope, the cylindrical and trapezoidal sources were bombarded with neutrons of differing energies to provide more favorable situations for specific isotopes. In particular, the neutrons used to activate the aluminum cylinders were lower in energy, to provide a favorable environment for neutron absorption that produces $^{28}_{13}$Al. In contrast, the trapezoids were subjected to high-energy neutrons which were more likely to knock nucleons off of the particles they collided with, which produced more $^{27}_{12}$Mg.

3 Data Collected

For all data collection done in the lab, the HV power supply was set to 810 V with the amplifier gain set to 39.

3.1 Calibration Data

Before any actual data was collected, a long measurement was taken of the emission spectrum from both sourceless background radiation, and sources with known emissions. This was then used to calibrate the software and subsequently determine the locations of the photo-peaks expected from the activated aluminum sources by correlating observed photo-peaks with the emission spectra of previously investigated sources. The data used for calibration is shown in Table 2, and the values then calculated for the expected photo-peaks are shown in Table 3.

Energy	Channel Number	Source
662 keV	302	^{137}Cs
1173 keV	522	^{60}Co
1332 keV	591	^{60}Co
1461 keV	645	^{40}K (background)

Tab. 2: Calibration Data: Channel Number $= 0.43$(Energy in keV) $\pm\, 0.0012 + 17.5 \pm 1.5$

The photo-peak in background radiation from ^{232}Th in the environment was not measured, because it was too weak to reliably determine peak bounds[1]. Note that this data is sufficient, as only the photo-peak's position is relevant to calculating the half lives of the specimens of interest. For a graphical representation of the relationship between photon energy and channel number, the data in Table 2 has been rendered into Figure 8 in the Appendix B.

Energy (keV)	Channel Number	Source
843 keV	380	^{27}Mg
1014 keV	454	^{27}Mg
1779 keV	782	^{28}Al

Tab. 3: Channels Calculated for Expected Photo-peaks

The channel number values in Table 3 were calculated using the relation derived by Maestro from the calibration data in Table 2, and rounding the result to the nearest integer value. A weighting system could have been implemented

[1] Professor Cecil identified this as an issue with the detector and advised against attempting to reconcile a ^{232}Th peak with other calibration data. It is also the reason for the double-sources described in Section 3.2.

to account for the non-integer values produced, but this was deemed unnecessary because measurements were to be taken over a region that would include a multitude of channels encompassing those that bounded the calculated values. In particular, to accommodate the short half-lives of the specimens produced in the activated aluminum regions of interest were prepared beforehand using the 32 closest channels on either side of the calculated channels in Table 3. This region width was decided upon by finding the mean of the observed photo-peaks in the calibration data, as we expect the photo-peaks of interest to be similarly-sized[2]. An image of the spectrum observed for the calibration sources is given in Figure 9 in Appendix B

3.2 Activated Aluminum Data

The first set of measurements taken used the cylindrical, activated aluminum sources described in Section 2.2. Due to previously-mentioned issues with the detector used, two cylinder sources were simultaneously placed in front of the detector. Initially, the hope was that by measuring only the cylinder sources, data could be reliably gathered on all three photo-peaks. As illustrated in Section 4, this was not the case. Data was nonetheless gathered for all three peaks, and is shown in Table 4. Images of the first and last spectrum measured for this source are shown in Figure 10 in Appendix B to help summarize why certain peak data may be more reliable than others.

Time (seconds from start)	**Net Areas of Photo-peaks**		
	843 keV	**1014 keV**	**1461 keV**
0	465 ±99	-10 ±91	613 ±64
94	586 ±86	122 ±75	382 ±57
182	371 ±88	118 ±67	266 ±44
249	515 ±76	54 ±71	119 ±43
327	299 ±84	154 ±56	167 ±40
396	260 ±80	94 ±60	81 ±41
462	270 ±78	27 ±66	25 ±49
543	160 ±80	44 ±63	49 ±44
632	147 ±79	193 ±52	63 ±35
710	136 ±78	-58 ±66	89 ±23
782	243 ±74	8 ±61	24 ±34
852	202 ±76	81 ±56	37 ±35
918	157 ±73	16 ±61	59 ±27
986	148 ±69	-87 ±67	46 ±27
1054	114 ±74	20 ±60	11 ±38
1125	205 ±68	3 ±60	-46 ±48
1196	-47 ±80	32 ±59	15 ±38

Tab. 4: Data Collected from Activated Aluminum Cylinder

This data set was taken with Maestro's data collection routine set to stop after 60 seconds "live time". Live time refers to the time spent by hardware actually collecting data, or equivalently the amount of real time that passed minus the processing latency of the hardware. The first measurement was taken immediately when the sources were placed, and all other measurements are labeled with the total amount of time that had elapsed since taking that first measurement.

The second set of measurements were taken using the activated aluminum trapezoids described in Section 2.2 and are shown in Table 5. As with the cylinders, two sources were placed in front of the detector rather than one. For consistency's sake alone, measurements were again taken of all three photo-peaks. Images of the first and last spectrum measured for this source are shown in Figure 11 in Appendix B to help summarize why certain peak data may be more reliable than others.

Time (seconds from start)	Net Areas of Photo-peaks		
	843 keV	**1014 keV**	**1461 keV**
0	2293 ±156	563 ±132	102 ±92
152	1823 ±148	492 ±128	163 ±87
286	1759 ±141	459 ±123	126 ±85
422	1316 ±142	459 ±117	-114 ±104
568	1133 ±140	490 ±117	-51 ±102
700	859 ±138	159 ±126	254 ±74
834	838 ±130	78 ±125	-18 ±95
975	739 ±130	410 ±107	144 ±87
1109	756 ±124	-18 ±124	175 ±81
1241	438 ±128	113 ±117	44 ±93
1375	676 ±119	-38 ±121	197 ±78
1509	320 ±129	11 ±121	-270 ±114
1647	312 ±126	-24 ±120	-103 ±104
1782	412 ±119	-158 ±123	-22 ±99
1932	211 ±127	160 ±111	30 ±93
2095	68 ±128	-113 ±122	11 ±93
2238	189 ±119	-126 ±122	-42 ±98
2381	63 ±124	-39 ±117	71 ±90
2519	-63 ±124	139 ±109	19 ±94

Tab. 5: Data Collected from Activated Aluminum Trapezoids

These measurements were taken after first setting Maestro's presets to stop collecting data after 120 seconds of live time.

All measurements and associated error are shown as reported by Maestro. Recall that the Net Area refers to the total number of counts in a region minus the background calculated by summing the counts in the first and last three channels of the region. For extra information, see Appendix C.

4 Data Analysis

4.1 Model

Radioactive particles undergo a statistical decay that follows

$$N[t] = N_0 e^{-\lambda t} \tag{1}$$

Where $N[t]$ is the number of particles in the sample at a time t, N_0 is the initial number of particles (i.e. $N[0]$) and λ is the probability that any given particle will decay at any given moment[1]. Assuming a large enough sample, the rate of decays can be modeled as linearly proportional to the intensity of a spherically symmetrical distribution of radiated photons. Therefore, the number of radioactive particles remaining in the sample can be directly related to the count rate of photons incident on a detector. The proportionality constant would be applied both to $N[t]$ and N_0. Therefore it is common to both sides of Eqn. 1 and can be divided off of the equation. Thus the count rate of photons emitted from a sample of radioactive particles can be modeled as

$$C[t] = C_0 e^{-\lambda t} \tag{2}$$

where $C[t]$ is the count rate at any given time and C_0 is the initial count rate. Notice that Eqn. 2 can easily be solved for the time in the special case that $C[t] = \frac{1}{2}C_0$, immediately yielding an expression for the half-life of a sample.

$$T_{1/2} = \frac{\ln[2]}{\lambda} \tag{3}$$

4.2 Exponential Fits to Experimental Data

In order to obtain trend curves and potential values for λ - and by extension $T_{1/2}$ - least squares analyses were performed on each collected data set for both sources in an attempt to fit them to Eqn. 2. Because presets in the

data collection software ensured that all measurement intervals were the same duration, the total number of counts of radiated photons in those intervals are proportional to the count rate in that time period. Therefore the direct Net Area values provided by Maestro were plotted.

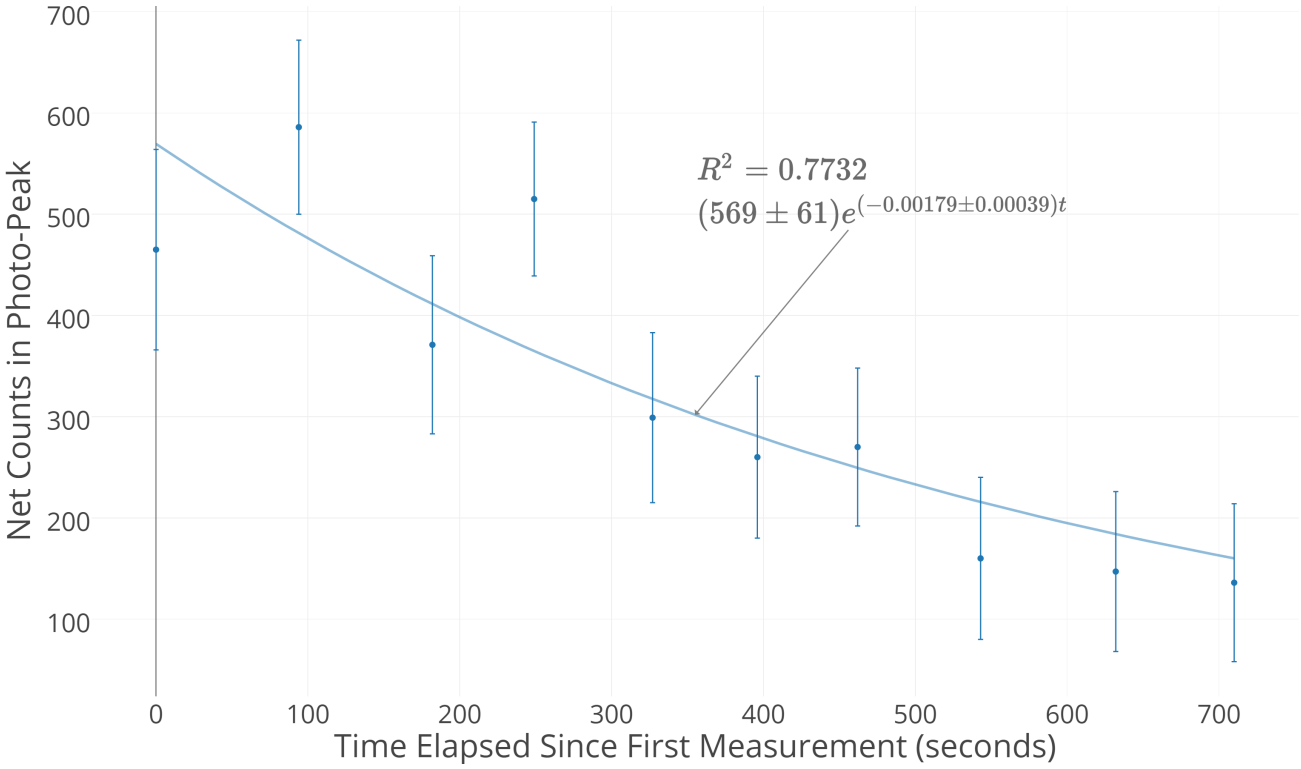

Fig. 2: Net Area of 843 keV Photo-Peak from Cylindrical Source

Figure 2 shows a fit of the data collected for the 843 keV photo-peak using a cylindrical source. The plot excludes data points obtained after 710 seconds because they begin to fluctuate seemingly randomly between 100 and 240 net area, and the last data point reports a net area under background levels. After this admittedly aggressive exclusion policy, a somewhat acceptable fit has been made. R^2 sits at a passing grade of 77.32% and the errors of the free parameters are both an order of magnitude under the values themselves.

Figure 3 shows a model fit for data collected from a cylindrical aluminum source at the 1014 keV photo-peak. Contrary to Figure 2, negative-valued data points are not excluded here for the simple reason that this data is too anomalous to fix by omitting any obvious outliers. The low R^2 value indicates that this data does not fit the model very well, but a more intuitive metric might be to notice what this implies numerically about the errors associated with the free parameters of the fit. The coefficient on the exponential meant to represent the initial net area has an error of more than 46% of its value, and even if it were to err maximally ($C_0 = 139$) it comes nowhere near being the maximum value, and as the earliest point in the decay data it ought to be the maximum value. Likewise, the decay constant has an error that is a staggering $83.\bar{3}\%$ of its value.

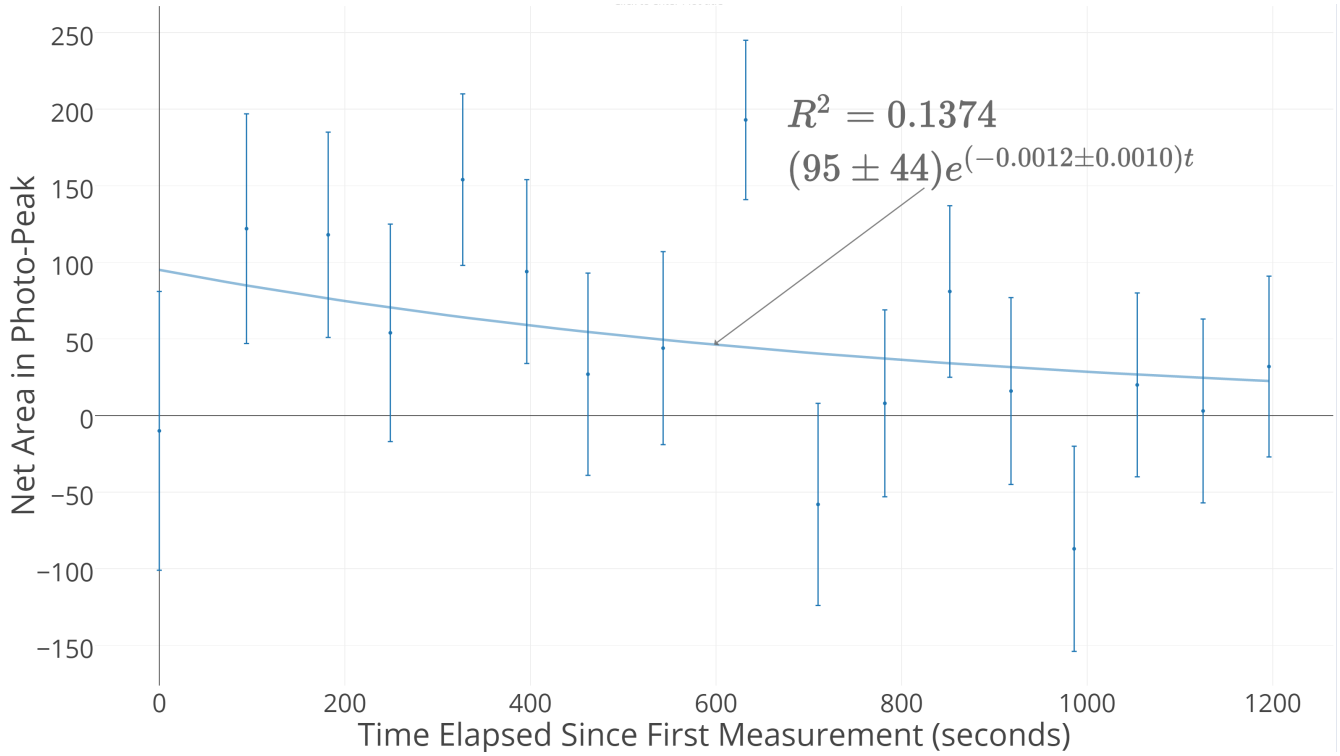

Fig. 3: Net Area of 1014 keV Photo-Peak from Cylindrical Source

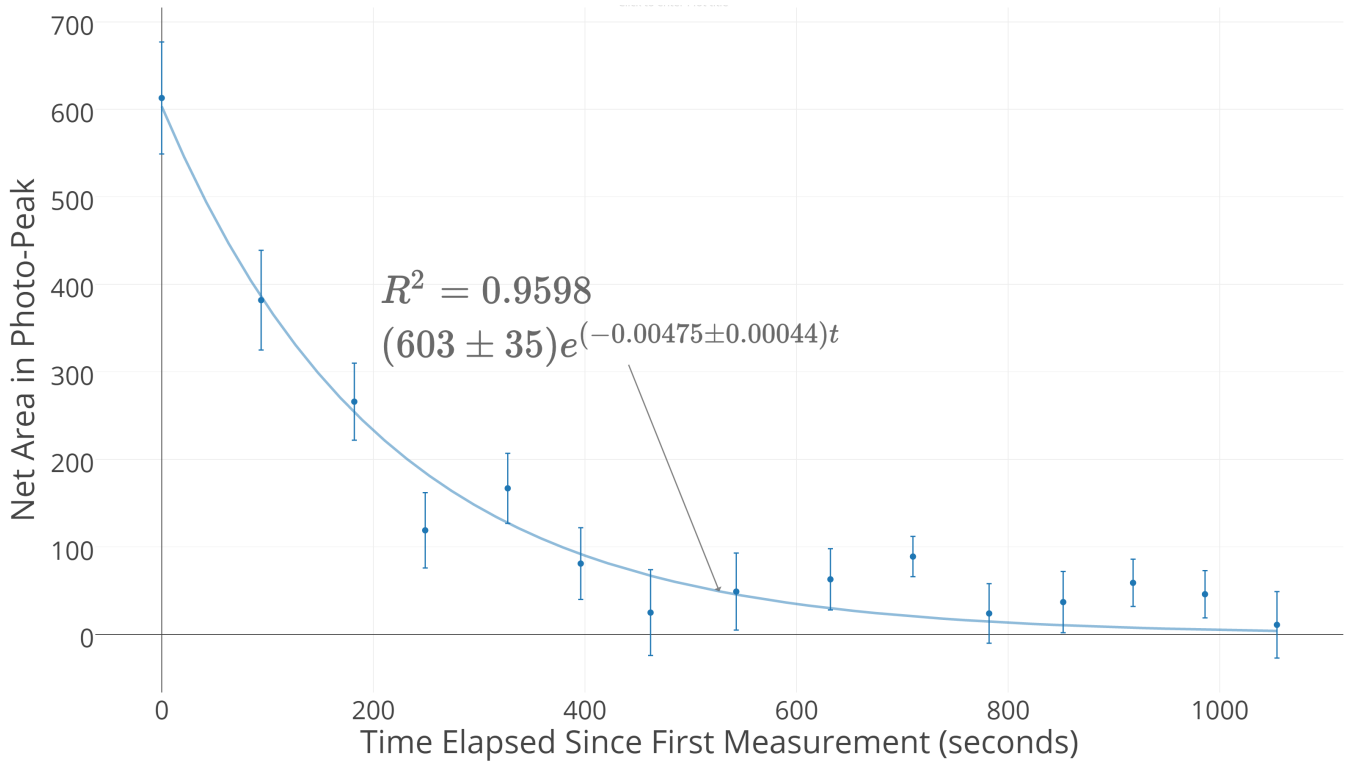

Fig. 4: Net Area of 1779 keV Photo-Peak from Cylindrical Source

Figure 4 shows the best fit yet, using data from the 1779 keV photo-peak of a cylindrical activated aluminum source. The R^2 of the fit is very close to 1, despite the odd periodicity exhibited at the far right of the plot. This plot omits the final two data points from Table 4 because not only had the magnitude of the error become greater

than the magnitude of the net area data points themselves, but the very next datum collected showed a negative value.

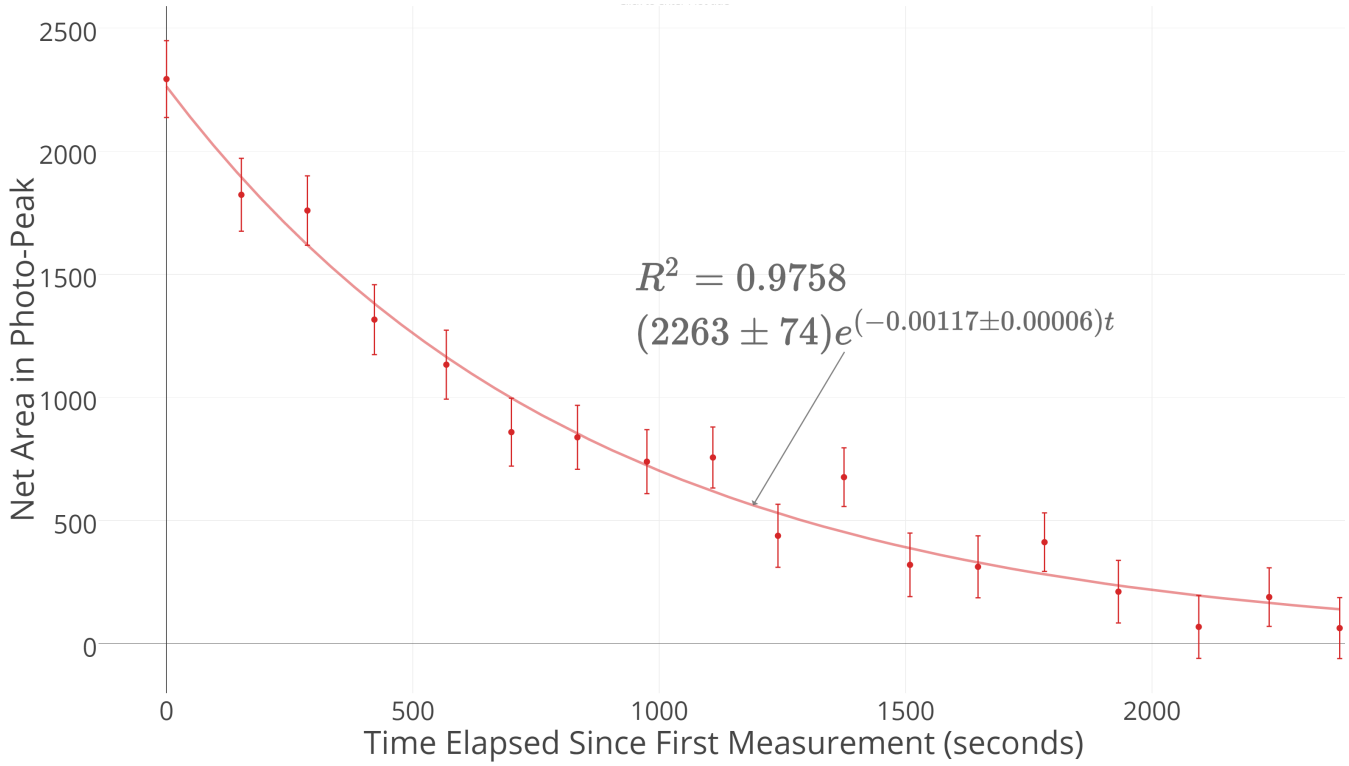

Fig. 5: Net Area of 843 keV Photo-Peak from Trapezoidal Source

Fortunately the 843 keV photo-peak data collected from the trapezoid source provides a close fit to the model, because the data from the cylindrical source did not. The final two data points from Table 5 have been omitted because the error became roughly double the magnitude of the value, and a negative value indicating no peak to speak of was reported.

Figure 6 shows a pretty rough fit to the model, but consider that the effect of propagating this error to the exponential leaves an error of 25% of the fit value. By contrast, the error in the exponential's coefficient is close to 15% of the fit value. So the closeness of the fit in this case may not be a good indicator that a half life calculated from this fit will produce a value close to the expected one. In fact, negative data points were not omitted in this plot because it actually degraded the quality of the fit, and no single application of a Q-test afterward could rectify this.

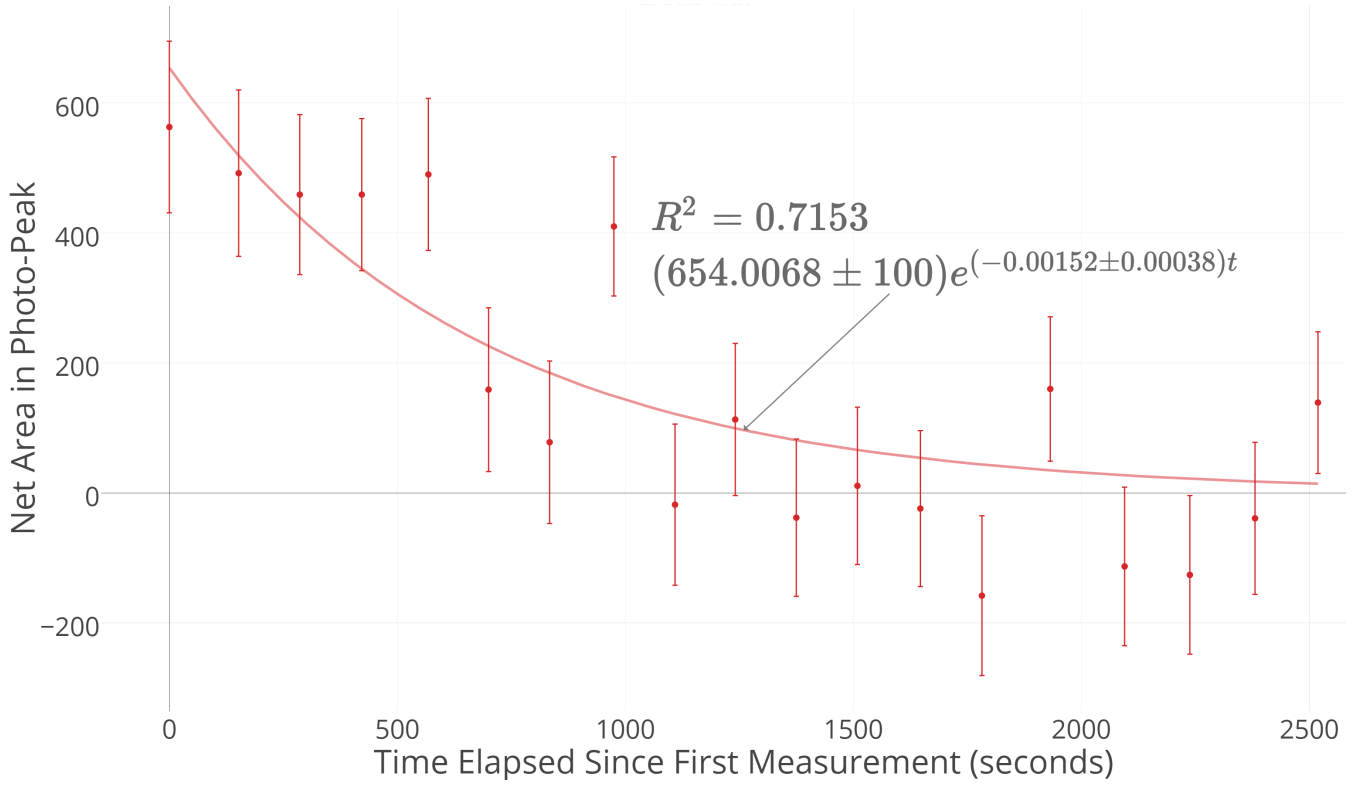

Fig. 6: Net Area of 1014 keV Photo-Peak from Trapezoidal Source

Similar to Figure 3, Figure 7 is shown primarily to illustrate that a least squares fit of this data does not provide a good fit to the model. This is the worst fit of all 6, in fact, with an error in the fit's decay constant that actually eclipses the value itself.

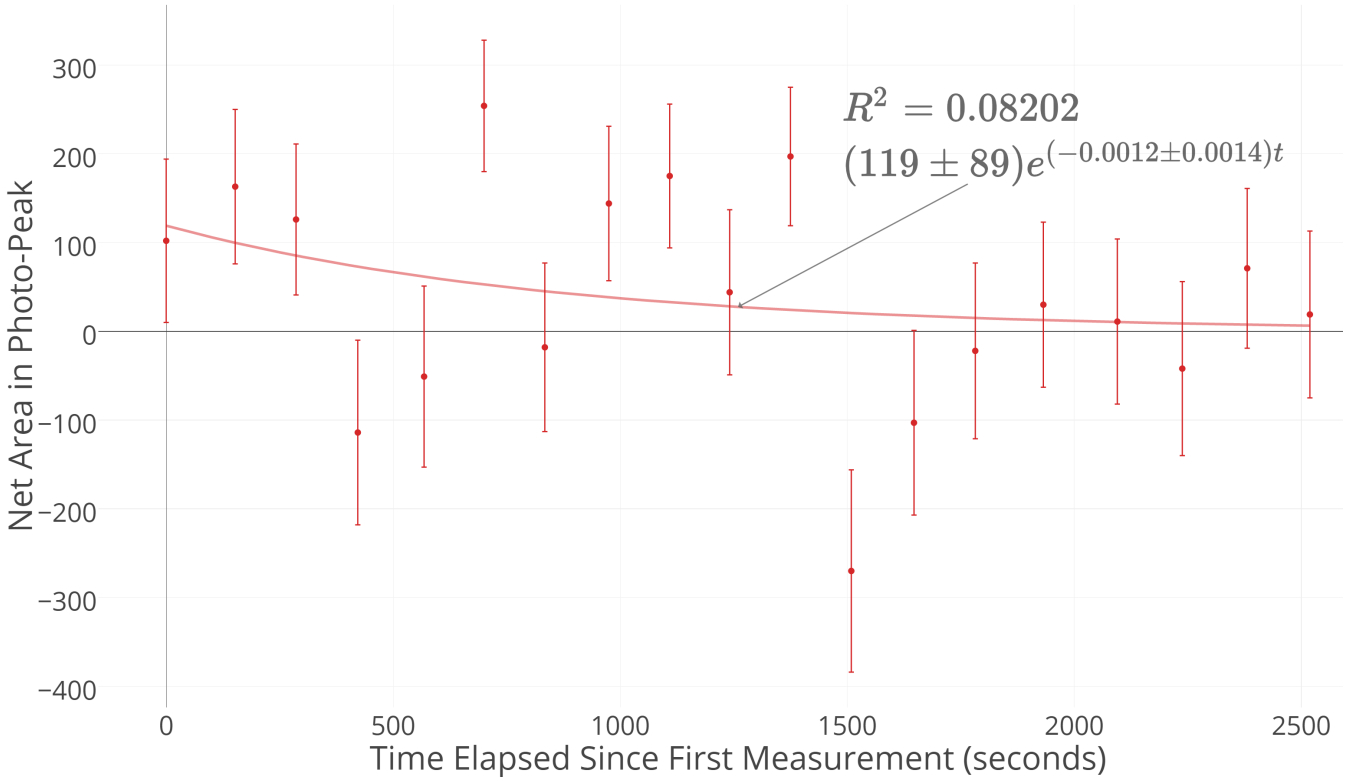

Fig. 7: Net Area of 1779 keV Photo-Peak from Trapezoidal Source

4.3 Fixed-Coefficient Averages

In addition to the fit values, averages were taken of values for the decay constant calculated at each point in each data set. The coefficients of the exponentials in the model (Refer to 4.1) for each calculated value were fixed to represent the initial net area in the photopeak. Generally speaking, this means the value of the net area at $t = 0$, but if an exception was made it will be mentioned. Of course, all negative-valued data points were excluded because they make a logarithm in their calculation impossible.

Error was calculated by propagating error from each measurement to the calculation of λ. Specifically, by solving Eqn. 2 for λ the following expression was obtained

$$\lambda = \frac{\ln(\frac{C_0}{C})}{t} \tag{4}$$

and the error was found to be[3]

$$\Delta\lambda = \sqrt{\left(\frac{\delta\lambda}{\delta C}\right)^2 (\Delta C)^2 + \left(\frac{\delta\lambda}{\delta C_0}\right)^2 (\Delta C_0)^2} = \frac{\sqrt{\left(\frac{\Delta C}{C}\right)^2 + \left(\frac{\Delta C_0}{C_0}\right)^2}}{t} \tag{5}$$

where the error in the measurement of time is considered insignificant in the face of huge net area errors in the photo-peaks, since timing error essentially comes down to circuit delay. To see in detail how this error propagates to the average value's error, see Appendix A.

4.3.1 Cylindrical Source Data

The average calculated decay constants for the cylindrical source are listed in Table 6. For the 843 keV photo-peak, the last point was not used because it was negative and the first data point was not used as C_0 because it was not the maximum value in the collection. Instead, C_0 was calculated by solving Eqn. 2 for C_0, using the second data point's $C[t]$ and $[t]$, and using the accepted value for λ. (Thus for error analysis, the error in C_0 is identical to the error in $C[94\ s]$)

Photo-Peak Energy	Average Decay Constant (Hz)
843 keV	0.00216 ±0.00023
1779 keV	0.00479 ±0.00045

Tab. 6: Average Decay Constants (Calculated from Cylindrical Source Data)

Note that due to poor data quality (many negatives, lack of recognizable trend etc.), values were not calculated for the 1014 keV photo-peak.

4.3.2 Trapezoidal Source Data

The average calculated decay constants for the trapezoidal source are listed in Table 7.

Photo-Peak Energy	Average Decay Constant (Hz)
843 keV	0.00124 ±0.00010
1014 keV	0.00109 ±0.00075

Tab. 7: Average Decay Constants (Calculated from Trapezoidal Source Data)

The 1779 keV data is not represented here due to it not only being half composed of negative values, but the poor relation between the positive data and the model. Notice that the error of the average 1014 keV value is nearly as large as the value itself. This is primarily because the exclusion of negative values favors earlier data points which have unusually high values and also causes the latter two-thirds of the collected data to take on very arbitrary, random pattern of oscillation between about 0 and 175 (see Figure 6 for visual aid).

4.4 Results Compared to Expected Values

The accepted values for the half-lives of ${}^{27}_{1}2\text{Mg}$ and ${}^{28}_{13}\text{Al}$ are 9.458 minutes = 567.48 seconds and 2.2414 minutes = 134.484 seconds, respectively[4]. The best candidates for each of these is found by converting decay constants to half lives via Eqn. 3, and the errors are given by[3]

$$\Delta T_{1/2} = \sqrt{\left(\frac{\delta T_{1/2}}{\delta \lambda}\right)^2 (\Delta\lambda)^2} = \frac{\ln(2)\Delta\lambda}{\lambda^2}. \tag{6}$$

The values in question are shown in Table 8

Specimen	Experimental $T_{1/2}$ Value (seconds)
${}^{27}_{12}\text{Mg}$	592 ±30.4
${}^{28}_{13}\text{Al}$	145 ±13.6

Tab. 8: Closest Calculated Values to Accepted Values

$T_{1/2}$ was taken from the model fit in Figure 5. Actually, the calculated average value from Table 7 (843 keV) and the fit in Figure 3 were both closer, at and 561 ±45.1 s and 578 ±481 s respectively, but both were determined to have error values far too massive to be considered precise. Likewise, the ${}^{28}_{13}\text{Al}$ value - which was selected from the calculated average in Table 7 - had strong competition in the fit from Figure 4 at 146 ±13.5 s. To be fair, the value for ${}^{27}_{12}\text{Mg}$ requires letting C_0 vary from the measured values, but for Figure 5 the entire range of C_0 is from 2189 to 2337, which fits well within the measured value's error range from 2137 to 2449. Therefore, allowing C_0 to vary in this manner is completely reasonable.

Note that the accepted value for the half-life of ${}^{27}_{12}\text{Mg}$ is 24.52 seconds less than the experimental value, which is within error, and the accepted value for the half-life of ${}^{28}_{13}\text{Al}$ is 10.516 seconds less than the experimental value, also within error.

5 Conclusion

It would appear that the trend of exponential decay can be reasonably preserved, even when data collection periods approach significant fractions of the isotope's half-life. In particular, it was somewhat surprising that the closest match to the accepted value for $^{28}_{13}$Al's half-life came from data collected over periods that were roughly 50% of it's half-life. The far greater issue came from attempting to resolve measurements that approached background noise; in several cases I discussed how outliers (especially negative values) were excluded from calculations because they were highly disruptive to the data. Making shorter measurements *would* help, but only because they keep error from approaching the same magnitude in the values themselves.

Furthermore, it was surprising how drastic an effect the energy of the neutrons used to activate the aluminum samples could have. By this I mainly mean that I expected the high-energy neutrons to occasionally "bounce" off of nuclei and lose energy, causing neutron absorption that would in turn cause the appearance of more $^{28}_{13}$Al than what was observed. In contrast to my expectations, the trapezoidal sources provided a worse fit to the model in the 1779 keV region than the cylindrical sources did in the 843 keV or 1014 keV regions. This was likely a result of the professor's attempt to make all photo-peaks measurable from the cylindrical sources, of course.

References

[1] Dr. Lawrence Wiencke, Professor for PHGN-326. A Brief Introduction to Nuclear Physics. Colorado School of Mines, Physics Department, 2017. http://astroserve.mines.edu/ph326/2017/lectures/1_Nuclear_326_post.pdf

[2] Dr. Ed Cecil, Professor for PHGN-326. Instructions for Experiments: Experiment 3: Neutron Activation. Colorado School of Mines, Physics Department, 2017.

[3] John R. Taylor, Professor at the University of Colorado Department of Physics."An Introduction to Error Analysis: The Study of Uncertainties in Physical Measurements" Second Edition, 1982.

[4] National Nuclear Data Center at the Brookhaven National Laboratory. "NuDat 2.6", Last Modification: 2011, http://www.nndc.bnl.gov/nudat2/chartNuc.jsp

A Uncertainty Calculation in Detail

What follows is a sample calculation of uncertainty in the average value calculated for the half-life of $^{28}_{13}$Al from the data in Table 4. The first step is to assume the model is of the form described in Section 4.1 and calculate this value for each data point. Naturally, this cannot be done at the time $t = 0$ because assuming that no decay has yet occurred destroys all information about the rate of decay. Because the first value measured for the net area is not the maximum of the data set, we cannot make the assumption that this first point is accurate and use it subsequently to determine C_0 for all other data points. Instead, since $t = 0$ cannot be used to determine a value for the half-life anyway, we threw it out and decided to make the assumption that a C_0 based on the second data point would be accurate. To do this, we solved Eqn. 2 for C_0 like so

$$C_0 = Ce^{\lambda t}$$

and used the accepted value for λ. This is equivalent to the assumption used in other data sets that the value measured at $t = 0$ is perfectly correct and corresponds exactly to C_0 (with some associated uncertainty, of course). The calculated value was

$$C_0 = 586e^{94*(\ln(2)/2.2414 \text{ minutes})} \approx 745$$

where the relation from Eqn. 3 was used to find an expression for λ in terms of the accepted $T_{1/2} = 2.2414$ minutes. The error in this value can be computed as simply the error in the second data point, considering that circuit delay uncertainty in time is an insignificant contribution to the total uncertainty. Therefore, the final value for C_0 in this data set is expressed as $C_0 = 745 \pm 86$. For each data point, a value for the decay constant was extracted by solving Eqn. 2 for λ:

$$C = C_0e^{-\lambda t} \rightarrow -\lambda t = \ln\left(\frac{C}{C_0}\right) \rightarrow \lambda = \frac{\ln\left(\frac{C_0}{C}\right)}{t}$$

Now, the final value we're interested in is an average of all of these, which is to say

$$\lambda_{\text{Avg.}} = \frac{\sum_{i=0}^{n}(\lambda_i)}{n},$$

and therefore we can find the uncertainty by decomposing it into a sum of contributions from each data point, so we're interested in the error at each data point. This can be calculated by propagating error from C and C_0 to λ in the following way:

$$\Delta\lambda = \sqrt{\left(\frac{\delta\lambda}{\delta C}\right)^2(\Delta C)^2 + \left(\frac{\delta\lambda}{\delta C_0}\right)^2(\Delta C_0)^2} = \frac{\sqrt{\left(\frac{\Delta C}{C}\right)^2 + \left(\frac{\Delta C_0}{C_0}\right)^2}}{t},$$

again assuming Δt is negligible. The values calculated from this are given in Table 9.

Time Elapsed Since First Measurement (seconds)	**Calculated λ (Hz)**
0	N/A
94	0.007105995848649 ±0.00193737770454
182	0.00565872477801 ±0.001074761664425
249	0.007366508936819 ±0.001510543093025
327	0.004573059345452 ±0.000799041097348
396	0.005603371372998 ±0.001305121396879
462	0.007347420765176 ±0.004248438793432
543	0.005012088250956 ±0.001664840334376
632	0.003908622613905 ±0.000894431514315
710	0.002992602603729 ±0.000392563310202
782	0.004393005611294 ±0.001816507195121
852	0.003524021485605 ±0.001117007159606
918	0.002762360320778 ±0.000511313350085
986	0.002824282780822 ±0.00060463455098
1054	0.003999515128635 ±0.003279053862848
1125	N/A (negative net area)
1196	0.003265329445884 ±0.002119969731035

Tab. 9: List of Calculated λs from 1779 keV Photo-Peak

As an intermediate step, significant figures are not considered at this stage. Now all that remains is to find the average, which is trivial, and the associated uncertainty, which is calculated in the following way:

$$\Delta\lambda = \sqrt{\sum_{i=0}^{n}\left[\left(\frac{\delta\lambda}{\delta\lambda_i}\right)^2(\Delta\lambda_i)^2\right]},$$

but of course every $\delta\lambda/\delta\lambda_i$ is just $1/n$, so this just leaves us with

$$\Delta\lambda = \frac{\sqrt{\sum_{i=0}^{n}\left[(\Delta\lambda_i^2)\right]}}{n} \approx 0.00045 \text{ Hz}$$

Of course, the actual value of interest is half-life, not decay constant. This is a simple conversion, though, and it follows directly from Eqn. 3 that the error in the half-life is expressed by

$$\Delta T_{1/2} = \sqrt{\left(\frac{\delta T_{1/2}}{\delta\lambda}\right)^2(\Delta\lambda)^2} = \frac{\ln(2)(\Delta\lambda)}{\lambda^2} \approx 13.6 \text{ seconds}$$

B Supplemental Figures

Note that Figures showing emission spectra from (or similar to) Maestro displays show a zoomed-in view of the spectrum to make the observed photo-peaks of interest easier to see. In figures that show spectra where a group of channels has been highlighted green, the highlighting is meant to show the approximate location of interesting photo-peaks and does *not* necessarily correspond exactly to a Maestro Region of Interest.

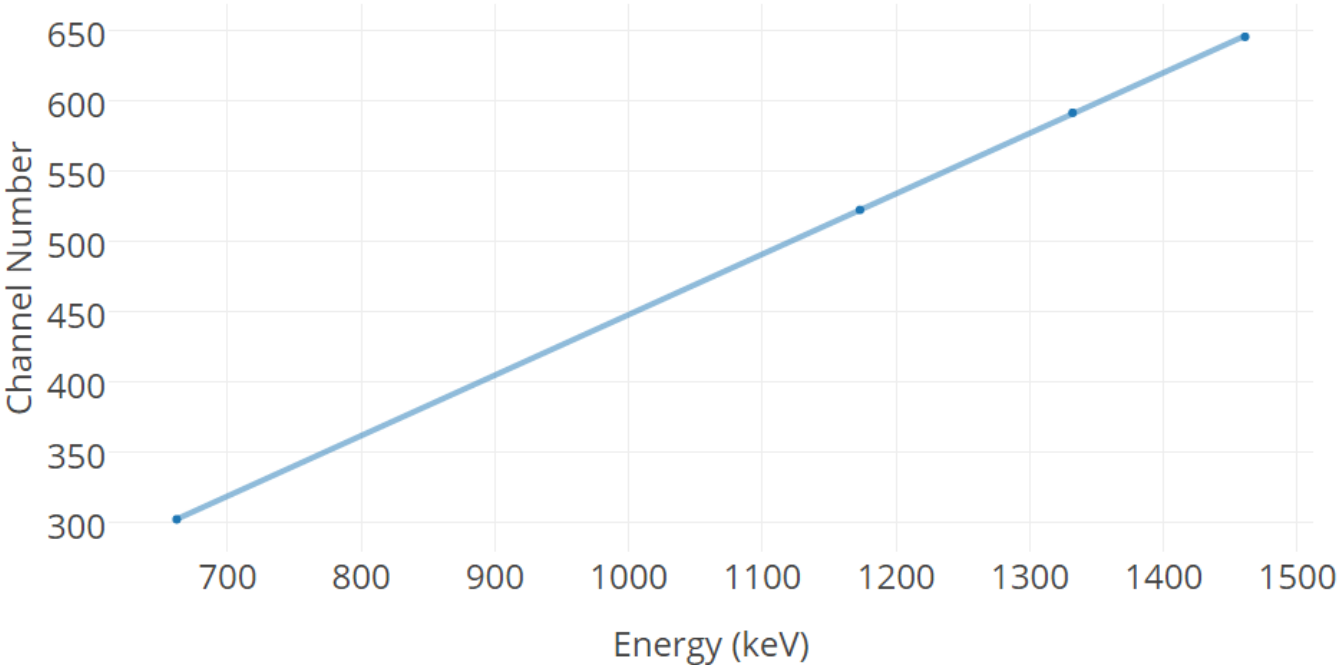

Fig. 8: Visual Representation of Calibration Data

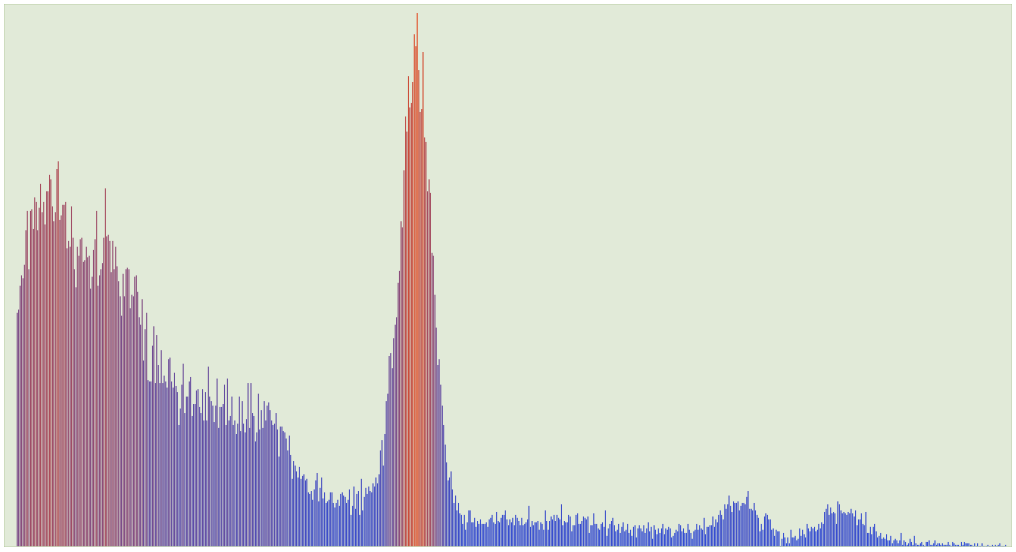

Fig. 9: Calibration Spectrum with ^{137}Cs and ^{60}Co Sources

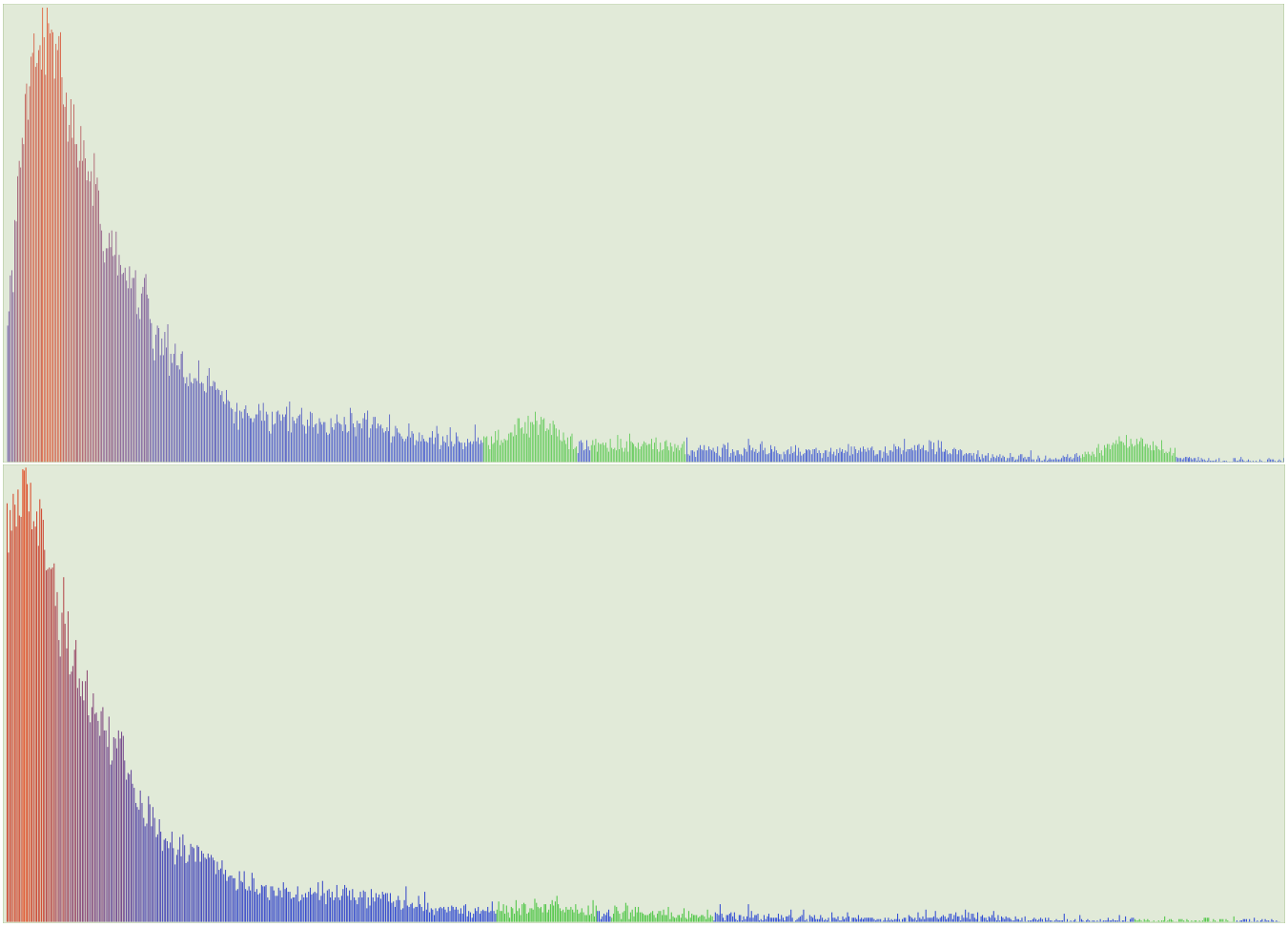

Fig. 10: Top: First Cylinder-Sourced Spectrum Collected, Bottom: Last Cylinder-Sourced Spectrum Collected

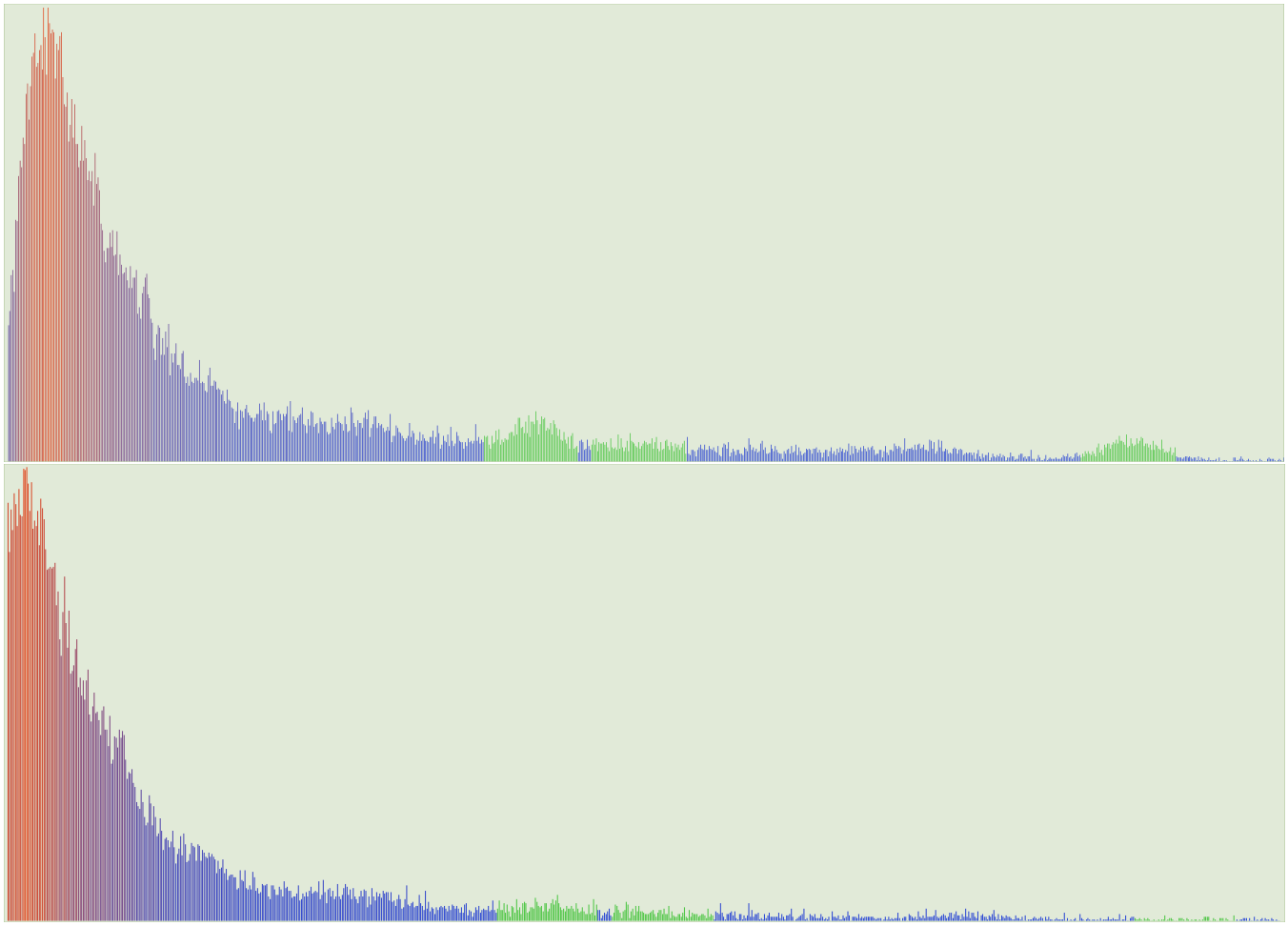

Fig. 11: Top: First Trapezoid-Sourced Spectrum Collected, Bottom: Last Trapezoid-Sourced Spectrum Collected

C Supplemental Information

Elapsed times in Tables 4 and 5 are shown as real time. Due to this and also due to the time required to record all three measurements then start another collection process as well as the limitations of human reaction time, the recorded times are accurate, though they do not appear close to the preset live time in separation. the first measurement of the first data set (that is, the data collected from the cylindrical source) occurred at 09:11:09 AM on the date of the experiment, and the first measurement of the second data set (that is, the data collected from the trapezoidal source) occurred at 9:51:43 AM the same day. Data collected is being retained in `.Spe` ASCII format (which preserves date/time of measurement and even live/real time spent) for the remainder of the semester, and is available upon request (not included here because data file length considered wasteful).